NASA-CR-199969

FINAL

IN-63-CR

0 CIT.

7048

P. 14

Final Report

University Consortium Agreement #NCC2-5012

(NASA-CR-199969) CONTROL THEORY BASED AIRFOIL DESIGN FOR POTENTIAL FLOW AND A FINITE VOLUME DISCRETIZATION (Princeton Univ.) 14 p

N96-16913

Unclas

G3/63 0091297

Principal Investigator: Prof. M. Hafez
Dept. of Mechanical and Aero Engineering
U C Davis, Davis, CA
December 1995

NCC 2-5012

Control Theory Based Airfoil Design for Potential Flow and a Finite Volume Discretization

*J. Reuther** and *A. Jameson*†
Department of Mechanical and Aerospace Engineering
Princeton University
Princeton, New Jersey 08544, U.S.A.

Abstract

This paper describes the implementation of optimization techniques based on control theory for airfoil design. In previous studies [6, 7] it was shown that control theory could be used to devise an effective optimization procedure for two-dimensional profiles in which the shape is determined by a conformal transformation from a unit circle, and the control is the mapping function. The goal of our present work is to develop a method which does not depend on conformal mapping, so that it can be extended to treat three-dimensional problems. Therefore, we have developed a method which can address arbitrary geometric shapes through the use of a finite volume method to discretize the potential flow equation. Here the control law serves to provide computationally inexpensive gradient information to a standard numerical optimization method. Results are presented, where both target speed distributions and minimum drag are used as objective functions.

Nomenclature

A_{ij}	grid transformation coefficients
b	design variable
B	generic co-state variable
c	speed of sound
C	bounding surface of flowfield domain on airfoil
C_d	coefficient of drag
C_l	coefficient of lift
C_p	coefficient of pressure
C_p^*	coefficient of pressure for sonic flow
d	modulus of conformal mapping transformation
D	flowfield domain
f	control law, control parameter
G	generic flowfield variable
h	Jacobian of generalized transformation
H	grid transformation matrix
I	cost function
J	grid transformation matrix
m	number of flowfield evaluations per line search
M	local Mach number
M_∞	Mach number at infinity
n	number of design variables
p	pressure
P	grid perturbation variational
q	speed
q_d	desired speed
q_∞	speed at infinity
Q	grid perturbation variational
R	generic governing equation for flowfield
s	arc length along airfoil surface
S	modified boundary condition for ψ
t_1, t_2	exponents on basis functions
u, v	Cartesian velocity components
U, V	contra-variant velocity components
x, y	Cartesian coordinates
X	physical position in flowfield
ξ, η	body fitted coordinates
α	angle of attack
ϕ	velocity potential
γ	ratio of specific heats
ψ	co-state variable for potential flow
ρ	density
θ	angle around circle

*Graduate Student, Student Member AIAA
†James S. McDonnell Distinguished University Professor of Aerospace Engineering, AIAA Fellow

Copyright ©1994 by the American Institute of Aeronautics and Astronautics, Inc. All rights reserved

Formulation of the design problem as a control problem

Ultimately, the designer seeks to optimize the geometric shape of a configuration taking into account the trade-offs between aerodynamic performance, structure weight, and the requirement for internal volume to contain fuel and payload. The subtlety and complexity of fluid flow is such that it is unlikely that repeated trials in an interactive analysis and design procedure can lead to a truly optimum design. Progress toward automatic design has been restricted by the extreme computing costs that might be incurred from brute force numerical optimization. However, useful design methods have been devised for various simplified cases, such as two-dimensional airfoils in viscous flows [13] and wings in invicid flows. The computational costs for these methods result directly from the vast number of flow solutions that are required to obtain a converged design.

Alternatively, it has been recognized that the designer generally has an idea of the kind of pressure distribution that will lead to the desired performance. Thus, it is useful to consider the inverse problem of calculating the shape that will lead to a given pressure distribution. The method is advantageous, since only one flow solution is required to obtain the desired design. Unfortunately, a physically realizable shape may not necessarily exist, unless the pressure distribution satisfies certain constraints, thus the problem must be very carefully formulated.

The problem of designing a two-dimensional profile to attain a desired pressure distribution was first studied by Lighthill, who solved it for the case of incompressible flow with a conformal mapping of the profile to a unit circle [9]. The speed over the profile is

$$q = \frac{1}{d}\,|\nabla\phi|$$

where ϕ is the potential which is known for incompressible flow and d is the modulus of the mapping function. The surface value of d can be obtained by setting $q = q_d$, where q_d is the desired speed, and since the mapping function is analytic, it is uniquely determined by the value of d on the boundary. A solution exists for a given speed q_∞ at infinity only if

$$\frac{1}{2\pi}\oint q\,d\theta = q_\infty,$$

and there are additional constraints on q if the profile is required to be closed.

The difficulty that the objective may be unattainable can be circumvented by regarding the design problem as a control problem in which the control is the shape of the boundary. A variety of alternative formulations of the design problem can then be treated systematically within the framework of the mathematical theory for control of systems governed by partial differential equations [10]. This approach to optimal aerodynamic design was introduced by Jameson [6, 7], who examined the design problem for compressible flow with shock waves, and devised adjoint equations to determine the gradient for both potential flow and also flows governed by the Euler equations. More recently Ta'asan, Kuruvila, and Salas, implemented a one shot approach in which the constraint represented by the flow equations is only required to be satisfied by the final converged solution [16]. Pironneau has also studied the use of control theory for optimum shape design of systems governed by elliptic equations [12].

Suppose that the boundary is defined by a function $f(\mathbf{x})$, where $\mathbf{x}$ is the position vector, and the desired objective is measured by a cost function I. This may, for example, measure the deviation from a desired surface pressure distribution, but it can also represent other measures of performance such as lift and drag. Thus, the problem is recast into a numerical optimization procedure in which the computationally expensive finite difference gradient of the objective function with respect to the control or design variables is replaced by the first variation in the cost function. Suppose that a variation δf in the control produces a variation δI in the cost.

For flow about an airfoil the aerodynamic properties which define the cost function are functions of the flow-field variables (G) and the physical location (X);

$$I = I(G, X).$$

Thus,

$$\delta I = \frac{\partial I}{\partial G}\delta G + \frac{\partial I}{\partial X}\delta X. \qquad (1)$$

As pointed out by Baysal and Eleshaky [1] each term in (1), except for δG, can be easily obtained. $\frac{\partial I}{\partial G}$

and $\frac{\partial I}{\partial X}$ can be obtained directly without a flowfield evaluation since they are partial derivatives. δX can be determined for each design variable by succesive grid generation so long as this cost is significantly less then the cost of the flow solution. δG traditionally requires a flowfield evaluation for each design variable independantly (brute force gradient methods). Here we introduce the governing equations of the flowfield as a constraint in such a way that the flowfield evaluation is eliminated from the expression for the gradient. Like the cost function, the governing equation R is a function of G and X within the flowfield domain D,

$$R = R(G, X) = 0.$$

Thus,

$$\delta R = \frac{\partial R}{\partial G}\delta G + \frac{\partial R}{\partial X}\delta X = 0. \tag{2}$$

Next, using a Lagrange Multiplier B we have

$$\delta I = \frac{\partial I}{\partial G}\delta G + \frac{\partial I}{\partial X}\delta X - B\left(\frac{\partial R}{\partial G}\delta G + \frac{\partial R}{\partial X}\delta X\right).$$

Choosing B such that,

$$\frac{\partial I}{\partial G} - B\frac{\partial R}{\partial G} = 0, \tag{3}$$

gives

$$\delta I = \frac{\partial I}{\partial X}\delta X - B\left(\frac{\partial R}{\partial X}\delta X\right). \tag{4}$$

The advantage is that (4) is independent of δG, therefore additional flowfield evaluations are not required to determine the gradient of I with respect to any number of design variables. The main cost is in solving the adjoint equation (3). In general, this adjoint problem is about as complex as a flow solution. If the number of design variables is large then the cost differential between one adjoint solution and many flowfield evaluations required to determine the gradient becomes compelling. Instead of intorducing a Lagrange multiplier, B, one can solve (2) for δG as

$$\delta G = -\left[\frac{\partial R}{\partial G}\right]^{-1}\frac{\partial R}{\partial X}\delta X,$$

and insert the result in (1). This is the implicit gradient approach, which is essentially equivalent to the control theory approach as has been pointed out by Shubin and Frank [14, 15].

After making such a modification, the gradient can be recalculated and the process repeated to follow a path of steepest descent until a minimum is reached. In order to avoid violating constraints, such as a minimum acceptable wing thickness, the gradient may be projected into the allowable subspace within which the constraints are satisfied. In this way one can devise procedures which must necessarily converge at least to a local minimum, and which can be accelerated by the use of more sophisticated descent methods such as conjugate gradient and quasi-Newton algorithms. There is the possibility of more than one local minimum, but in any case the method will lead to an improvement over the original design. Furthermore, unlike the traditional inverse algorithms, the cost function can be thought of as any measure of performance provided the adjoint system can be correctly formulated.

In the present method the steps to obtain (1 – 4) are applied to the governing differential equations rather than applying them to the corresponding discrete system. This latter approach is now gaining favor in the work of Newman and Tayor *et al.* [11, 8]. The two methods can be very similar, depending upon the discretization of (3). The current method has the advantage that the discretization and iteration scheme used to solve the flowfield system can also be applied directly to the adjoint system (4). In Jameson's previous application of control theory to optimal aerodynamic shape design a successful numerical implementation was demonstrated using a conformal transformation from a unit circle to generate the profile, so that the mapping function becomes the control. In this work, an alternative approach using a general coordinate transformation is adopted, and the equations are discretized by a finite volume method. This is intended to be a precursor for the three-dimensional problem, where conformal mapping is less suitable since it could be used only to provide independent transformations in separate planes.

Design for potential flow using finite volume discretization

Consider the case of two-dimensional compressible inviscid flow. In the absence of shock waves, an initially irrotational flow will remain irrotational, and we can assume that the velocity vector $\mathbf{q}$ is the gradient of a potential ϕ. In the presence of weak shock waves this remains a fairly good approximation.

Let p, ρ, c, and M be the pressure, density, speed-of-sound, and Mach number q/c. The potential flow equation is then

$$\nabla\cdot(\rho\nabla\phi) = 0, \tag{5}$$

where the density is given by

$$\rho = \left\{1 + \frac{\gamma-1}{2}M_\infty^2\left(1-q^2\right)\right\}^{\frac{1}{(\gamma-1)}}, \tag{6}$$

while

$$p = \frac{\rho^\gamma}{\gamma M_\infty^2}, \quad c^2 = \frac{\gamma p}{\rho}. \tag{7}$$

Here M_∞ is the Mach number in the free stream, and the equations have been non-dimensionalized so that ρ and q have the value unity in the far field.

The potential flow equation can be written

$$\frac{\partial}{\partial x}(\rho u) + \frac{\partial}{\partial y}(\rho v) = 0 \quad \text{in } D,$$

where u and v represent the cartesian velocity components. The coordinate transformations may be defined

$$\begin{bmatrix} u \\ v \end{bmatrix} = \begin{bmatrix} \phi_x \\ \phi_y \end{bmatrix} = \begin{bmatrix} \frac{\partial\xi}{\partial x} & \frac{\partial\eta}{\partial x} \\ \frac{\partial\xi}{\partial y} & \frac{\partial\eta}{\partial y} \end{bmatrix}\begin{bmatrix} \phi_\xi \\ \phi_\eta \end{bmatrix} = H^{T^{-1}}\begin{bmatrix} \phi_\xi \\ \phi_\eta \end{bmatrix}, \tag{8}$$

and also

$$\begin{bmatrix} \phi_\xi \\ \phi_\eta \end{bmatrix} = \begin{bmatrix} \frac{\partial x}{\partial\xi} & \frac{\partial y}{\partial\xi} \\ \frac{\partial x}{\partial\eta} & \frac{\partial y}{\partial\eta} \end{bmatrix}\begin{bmatrix} \phi_x \\ \phi_y \end{bmatrix} = H^T\begin{bmatrix} \phi_x \\ \phi_y \end{bmatrix},$$

where x and y represent the physical plane, and ξ and η represent the computational plane. By defining the Jacobian

$$h = \frac{\partial x}{\partial\xi}\frac{\partial y}{\partial\eta} - \frac{\partial x}{\partial\eta}\frac{\partial y}{\partial\xi},$$

we can write

$$\frac{\partial}{\partial\xi}(\rho h U) + \frac{\partial}{\partial\eta}(\rho h V) = 0 \quad \text{in } D. \tag{9}$$

Here, U and V represent the contravariant velocities

$$\begin{bmatrix} U \\ V \end{bmatrix} = \frac{1}{h}\begin{bmatrix} \frac{\partial y}{\partial\eta} & -\frac{\partial x}{\partial\eta} \\ -\frac{\partial y}{\partial\xi} & \frac{\partial x}{\partial\xi} \end{bmatrix}\begin{bmatrix} u \\ v \end{bmatrix} = H^{-1}\begin{bmatrix} u \\ v \end{bmatrix},$$

and

$$\begin{bmatrix} U \\ V \end{bmatrix} = H^{-1}H^{T^{-1}}\begin{bmatrix} \phi_\xi \\ \phi_\eta \end{bmatrix} = J^{-1}\begin{bmatrix} \phi_\xi \\ \phi_\eta \end{bmatrix}$$

with

$$J^{-1} = \begin{bmatrix} A_{11} & A_{12} \\ A_{12} & A_{22} \end{bmatrix}.$$

Thus,

$$U = A_{11}\phi_\xi + A_{12}\phi_\eta \tag{10}$$

$$V = A_{12}\phi_\xi + A_{22}\phi_\eta. \tag{11}$$

Consider first the case in which the cost function is defined such as to achieve a target speed distribution:

$$I = \frac{1}{2}\int_C (q-q_d)^2\,ds = \frac{1}{2}\int_C (q-q_d)^2\left(\frac{ds}{d\xi}\right)d\xi, \tag{12}$$

where q_d is the desired speed distribution and C is the airfoil surface.

The design problem is now treated as a control problem where the control function is the airfoil shape, which is to be chosen to minimize I subject to the constraints defined by the flow equations (5–11). The first variation of this cost function is

$$\begin{aligned} \delta I = & \int_C (q-q_d)\,\delta q\left(\frac{ds}{d\xi}\right)d\xi \\ & + \frac{1}{2}\int_C (q-q_d)^2\,\delta\left(\frac{ds}{d\xi}\right)d\xi \\ = & \int_C (q-q_d)\frac{\partial(\delta\phi)}{\partial\xi}d\xi \\ & + \frac{1}{2}\int_C (q-q_d)^2\,\delta\left(\frac{ds}{d\xi}\right)d\xi \\ & + \int_C (q-q_d)\frac{\partial\phi}{\partial\xi}\delta\left(\frac{d\xi}{ds}\right)\frac{ds}{d\xi}d\xi, \end{aligned} \tag{13}$$

since on the wall

$$q_w = \frac{\partial\phi}{\partial s} = \frac{\partial\phi}{\partial\xi}\frac{\partial\xi}{\partial s}.$$

In general we need to find how a modification to the airfoil geometry causes a variation $\delta\phi$, as well a variation in the grid parameters $\delta A_{11}, \delta A_{12}, \delta A_{22}$, and δh. Consider

$$\delta U = \delta(A_{11})\,\phi_\xi + A_{11}\delta\phi_\xi + \delta(A_{12})\,\phi_\eta + A_{12}\delta\phi_\eta$$

$$\delta V = \delta(A_{12})\,\phi_\xi + A_{12}\delta\phi_\xi + \delta(A_{22})\,\phi_\eta + A_{22}\delta\phi_\eta$$

$$\begin{aligned} \delta\rho = & -\frac{\rho}{c^2}\left[U\frac{\partial}{\partial\xi} + V\frac{\partial}{\partial\eta}\right]\delta\phi \\ & -\frac{\rho}{2c^2}\left[\delta A_{11}\phi_\xi^2 + 2\delta A_{12}\phi_\eta\phi_\xi + \delta A_{22}\phi_\eta^2\right]. \end{aligned}$$

It follows that $\delta\phi$ satisfies

$$L\delta\phi = -\frac{\partial}{\partial\xi}\left\{\begin{array}{c} \rho U\delta h \\ +\rho h\phi_\xi\left(1-\frac{U\phi_\xi}{2c^2}\right)\delta A_{11} \\ +\rho h\phi_\eta\left(1-\frac{U\phi_\xi}{c^2}\right)\delta A_{12} \\ +\rho h\phi_\eta\left(-\frac{U\phi_\eta}{2c^2}\right)\delta A_{22} \end{array}\right\}$$

$$-\frac{\partial}{\partial\eta}\left\{\begin{array}{c}\rho V\delta h\\ +\rho h\phi_\eta\left(1-\frac{V\phi_\eta}{2c^2}\right)\delta A_{22}\\ +\rho h\phi_\xi\left(1-\frac{V\phi_\eta}{c^2}\right)\delta A_{12}\\ +\rho h\phi_\xi\left(-\frac{V\phi_\xi}{2c^2}\right)\delta A_{11}\end{array}\right\},$$

or, defining the right hand side with P and Q,

$$\begin{aligned} L\delta\phi &= -\frac{\partial}{\partial\xi}Q\left(\delta h,\delta A_{11},\delta A_{12},\delta A_{22}\right)\\ &\quad -\frac{\partial}{\partial\eta}P\left(\delta h,\delta A_{11},\delta A_{12},\delta A_{22}\right) \quad (14)\end{aligned}$$

with

$$\begin{aligned} L = &\quad \frac{\partial}{\partial\xi}\left[\begin{array}{c}\rho h\left(A_{11}-\frac{U^2}{c^2}\right)\frac{\partial}{\partial\xi}\\ +\rho h\left(A_{12}-\frac{UV}{c^2}\right)\frac{\partial}{\partial\eta}\end{array}\right]\\ &+\frac{\partial}{\partial\eta}\left[\begin{array}{c}\rho h\left(A_{12}-\frac{UV}{c^2}\right)\frac{\partial}{\partial\xi}\\ +\rho h\left(A_{22}-\frac{V^2}{c^2}\right)\frac{\partial}{\partial\eta}\end{array}\right]. \quad (15)\end{aligned}$$

If ψ is any periodic function vanishing in the far field, equation (14) can be multiplied by ψ and integrated over the domain. After integrating the right hand side by parts we arrive at

$$\begin{aligned}\int_D \psi L\delta\phi d\xi d\eta = &\int_D \frac{\partial\psi}{\partial\xi}Q+\frac{\partial\psi}{\partial\eta}P\ d\xi d\eta\\ &+\int_C\left\{\psi\rho h\left[\delta A_{12}\phi_\xi+\delta A_{22}\phi_\eta\right]\right\}d\xi. \quad (16)\end{aligned}$$

Now subtracting (16) from (13),

$$\begin{aligned}\delta I = &-\int_C\frac{\partial\left(q-q_d\right)}{\partial\xi}\delta\phi d\xi\\ &+\int_C\frac{1}{2}\left(q-q_d\right)^2\delta\left(\frac{ds}{d\xi}\right)d\xi\\ &+\int_C\left(q-q_d\right)\frac{\partial\phi}{\partial\xi}\delta\left(\frac{d\xi}{ds}\right)\frac{ds}{d\xi}d\xi\\ &-\int_D\psi L\delta\phi d\xi d\eta\\ &+\int_D\frac{\delta\psi}{\delta\xi}Q+\frac{\delta\psi}{\delta\eta}P\ d\xi d\eta\\ &+\int_C\left\{\psi\rho h\left[\delta A_{12}\phi_\xi+\delta A_{22}\phi_\eta\right]\right\}d\xi.\end{aligned}$$

Then setting up the adjoint system we have

$$L\psi = 0 \quad \text{in } D, \qquad (17)$$

with the boundary condition

$$\rho h\left(A_{12}\psi_\xi+A_{22}\phi_\eta\right) = -\frac{\partial}{\partial\xi}\left(q-q_d\right). \qquad (18)$$

After appling the second form of Green's theorem to (17) we get

$$\begin{aligned}\int_D\psi L\delta\phi dS = &\int_C\left\{\psi\rho h\left[\delta A_{12}\phi_\xi+\delta A_{22}\phi_\eta\right]\right\}d\xi\\ &+\int_C\left\{\delta\phi\rho h\left[\delta A_{12}\psi_\xi+\delta A_{22}\psi_\eta\right]\right\}d\xi.\end{aligned}$$

Finally the variation can be defined as

$$\begin{aligned}\delta I = &\frac{1}{2}\int_C\left(q-q_d\right)^2\delta\left(\frac{ds}{d\xi}\right)d\xi\\ &+\int_C\left(q-q_d\right)\frac{\partial\phi}{\partial\xi}\delta\left(\frac{d\xi}{ds}\right)\frac{ds}{d\xi}d\xi\\ &+\int_D\frac{\partial\psi}{\partial\xi}Q+\frac{\partial\psi}{\partial\eta}P\ d\xi d\eta. \qquad (19)\end{aligned}$$

For this finite volume formulation no general analytic grid transformation is available. Furthermore, the variation with respect to the grid quantities is now spread into δA_{11}, δA_{12}, δA_{22}, and δh instead of just the modulus of the transformation as was the case for conformal mapping. Therefore, we adopted a more conventional method to construct δI. First, an independent basis space of perturbation functions $b(i)$, $i = 1,2,\ldots,n$ (n = number of design variables) is chosen that allows for the needed freedom of the design space. Thus, the shape f now becomes $f(b(i))$ with $b(i)$ being the control. Once δI is obtained, any optimization procedure can be employed to minimize the cost with respect to the given basis $b(i)$.

If the flow is subsonic, this procedure should converge toward the desired speed distribution since the solution will remain smooth, and no unbounded derivatives will appear. If, however, the flow is transonic, one must allow for the appearance of shock waves in the trial solutions, even if q_d is smooth. In such instances $q-q_d$ is not differentiable. This difficulty can be circumvented by a more sophisticated choice of the cost function. Consider the choice

$$I = \frac{1}{2}\int_C\left(\lambda_1 S^2+\lambda_2\left(\frac{dS}{d\xi}\right)^2\right)d\xi,$$

where λ_1 and λ_2 are parameters, and the periodic function $S(\xi)$ satisfies the equation

$$\lambda_1 S-\lambda_2\frac{d^2S}{d\xi^2} = q-q_d. \qquad (20)$$

Then,

$$\begin{aligned}\delta I &= \int_C\left(\lambda_1 S\,\delta S+\lambda_2\frac{dS}{d\xi}\frac{d}{d\xi}\delta S\right)d\xi\\ &= \int_C S\left(\lambda_1\,\delta S-\lambda_2\frac{d^2}{d\xi^2}\delta S\right)d\xi = \int_C S\,\delta q\,d\xi.\end{aligned}$$

Thus, S replaces $q-q_d$ in the previous formula and one modifies the boundary condition (18) to

$$\rho h\left(A_{12}\psi_\xi+A_{22}\phi_\eta\right) = -\frac{\partial}{\partial\xi}\left(S\right) \quad \text{on } C. \qquad (21)$$

For the case where the cost function is drag, (12) is replaced by,

$$I = \int_C p \frac{\partial y}{\partial \xi} d\xi. \tag{22}$$

The first variation of the cost function is now,

$$\begin{aligned} \delta I = & \int_C \delta p \frac{\partial y}{\partial \xi} d\xi \\ & + \int_C p \delta \left(\frac{\partial y}{\partial \xi} \right) d\xi \\ = & \int_C \frac{\partial \left(\rho q \frac{\partial y}{\partial s} \right)}{\partial \xi} \delta \phi d\xi \\ & - \int_C \rho q \frac{\partial \phi}{\partial \xi} \frac{\partial y}{\partial \xi} \delta \left(\frac{\partial \xi}{\partial s} \right) d\xi \\ & + \int_C p \delta \left(\frac{\partial y}{\partial \xi} \right) d\xi, \end{aligned} \tag{23}$$

Thus, (19) becomes

$$\begin{aligned} \delta I = & - \int_C \rho q \frac{\partial \phi}{\partial \xi} \frac{\partial y}{\partial \xi} \delta \left(\frac{\partial \xi}{\partial s} \right) d\xi \\ & + \int_C p \delta \left(\frac{\partial y}{\partial \xi} \right) d\xi \\ & + \int_D \frac{\partial \psi}{\partial \xi} Q + \frac{\partial \psi}{\partial \eta} P \, d\xi d\eta, \end{aligned} \tag{24}$$

where the boundary condition on ψ, (18) or (20), is replaced with

$$\rho h \left(A_{12} \psi_\xi + A_{22} \phi_\eta \right) = -\frac{\partial}{\partial \xi} \left(\rho q \frac{\partial y}{\partial s} \right) \tag{25}$$

or

$$\lambda_1 S - \lambda_2 \frac{d^2 S}{d\xi^2} = \rho q \frac{\partial y}{\partial s}. \tag{26}$$

The entire procedure can be summarized for the cost function based on target speed distribution as follows:

1. Solve the flow equations (5–11) for ϕ, u, v, q, ρ, U, and V.
2. Smooth the cost function if necessary by (20).
3. Solve the adjoint equation (15 and 17) for ψ subject to the boundary condition (18) or (21).
4. For each i independently perturb the design variables, $b(i)$, and calculate the necessary metric variations (δA_{11}, δA_{12}, δA_{22}, δh, and $\delta \left(\frac{ds}{d\xi} \right)$) by recalculating the perturbed grid with automatic grid generation.
5. Directly evaluate δI by equation (19).
6. Project δI into a feasible direction subject to any constraints to obtain $\delta \bar{I}$.
7. Feed $\delta \bar{I}$ as the gradient with respect to $b(i)$ to a quasi-Newton optimization procedure.
8. Calculate the search direction from the quasi-Newton algorithm and perform a line search.
9. Return to 1 if not converged.

In practice the method resembles those used by Hicks *et al.* [13] with the control theory replacing the brute force, finite difference based, gradient calculation. The current formulation has an advantage by requiring computational work proportional to $2+m$ flow solver evaluations (m being the number of calculations required per line search) per design cycle as opposed to $1 + m + n$. Thus, unlike conventional design optimization programs, the current method's computational cost does not hinge upon the number of design variables provided the grid regeneration is fast and automatic. The method also has the advantage of being quite general in that arbitrary choices for both the design variables and optimization technique are admitted. Finally, unlike the conformal mapping based method this approach can be directly extended to three-dimensions.

Implementation of the generalized potential flow design method

The practical implementation of the generalized potential flow design method, as with the conformal potential method, relies heavily upon fast accurate solvers for both the state (ϕ) and co-state (ψ) fields. Further, to improve the speed and realizability of the methods, a robust choice of the optimization algorithm must be made. Finally, appropriate design variables must be choosen which allow sufficient freedom in realizable designs. In this work, Jameson's FLO42 full potential computer program and the QNMDIF (by Gill, Murray and Wright [2]) quasi-Newton optimization algorithm are employed.

In FLO42 the flow solution is obtained by a rapid multigrid alternating direction method. The original scheme is described in [5]. The scheme uses artificial dissipative terms to introduce upwind biasing which simulates the rotated difference scheme [4] while preserving the conservation form. The alter-

nating direction method is a generalization of conventional alternating direction methods in which the scalar parameters are replaced by upwind difference operators to produce a scheme which remains stable as the equations change type from elliptic to hyperbolic in accordance with the flow becoming locally supersonic [5].

QNMDIF is an unconstrained quasi-Newton optimization algorithm that calculates updates to a Cholesky factored Hessian matrix by the DFP (Davidon-Fletcher-Powell) rank-two procedure. Hence, information about the curvature of the design space feeds in through the successive gradient calculations.

Since the primary computational costs arise from not only the flow solution algorithm but also the adjoint solution algorithm, both need to be computationally efficient. The adjoint equation has a form very similar to the flow equation. While it is linear in its dependent variable, it also changes type from elliptic (in subsonic zones of the flow) to hyperbolic (in supersonic zones of the flow). Thus, it was possible to adapt exactly the same algorithm to solve both the adjoint and the flow equations, but with reverse biasing of the difference operators in the downwind direction for the adjoint equation, corresponding to its reversed direction of the zone of dependence. A multigrid method is used to accelerate the convergence of a generalized alterating direction scheme in a manner similar to the flow solver.

Design variables are chosen with the following form, suggested by Hicks and Henne [3]:

$$b(x) = sin\left(\pi x^{\frac{log_{10}(.5)}{log_{10}(t_1)}}\right)^{t_2}$$

$$b(x) = x^{t_1}(1-x)e^{-t_2 x},$$

where t_1 and t_2 control the center and thickness of the perturbation and x is the normalized chord length.

When distributed over the entire chord on both upper and lower surfaces these analytic perturbation functions admit a large possible design space. They have the advantage of being space based functions, as opposed to frequency based functions, and thus they allow for local control of the design. They can be chosen such that symetry, thickness, or volume can be explicitly constrained. Further, particular choices of these variables will concentrate the design effort in regions where refinement is needed, while leaving the rest of the airfoil section virtually undisturbed. The disadvantage of these functions is that they do not form a complete basis space, nor are they orthogonal. Thus, they do not garantee that a solution, for example, of the inverse problem for a realizable target pressure distribution will necessarily be attained. Here they are employed due to their ease of use and ability to produce a wide variation of shapes with a limited number of design variables.

Numerical tests of the generalized potential flow design method

Several test cases are presented for the generalized potential flow design algorithm based on the finite volume scheme. These test cases can be catagorized into three basic groups. First, are non-lifting cases, where a symetric target pressure distribution is specified and the optimization is started from an arbitrary symetric initial guess.

The first non-lifting example shown in Figure 1, illustrates that for subsonic flow, $M_\infty = 0.2$ and $\alpha = 0°$, a given airfoil shape, in this case a NACA 64012, can be recovered by starting from an arbitrary shape and specifying the target pressure distribution. A close look at the final solution shows that a small discrepency is evident at the trailing edge. This may be associated with the lack of completness of our basis space. In the next example, see Figure 2, the design takes place at $M_\infty = 0.8$, $\alpha = 0°$, where the initial NACA 0012 airfoil is driven towards the subsonic pressure distribution of the NACA 64021. In this case the target pressure distribution exceeds Cp^* for $M_\infty = 0.8$. Therefore, the pressure distribution represents shock free transonic flow. Since, in general, such a pressure distribution may not be realizable, the program approaches the target with the nearest feasible pressure distribution. An examination of Figure 2 demonstrates that a very weak shock in the designed pressure distribution replaces the smooth transition to subsonic flow seen in the target distribution. In the final example non-lifting case of Figure 3, an arbitrary pressure distribution which does contain a shock wave and is realizable, is used as the target. Here the computer program was able to obtain the corresponding airfoil geometry along with the correct shock wave location with

a high degree of accuracy, as can be seen both in the pressure distribution and in the airfoils.

The second group of test cases address the problem of attaining a desired pressure distribution for lifting airfoils. The most convienient method of obtaining such solutions with the present design method is to determine the lift coefficient associated with the target pressure distribution, and match this lift with the initial airfoil. The design progresses with the flow solver and the adjoint system being driven by constant circulation instead of fixed angle of attack. The first example using this technique, shown in Figure 4, drives the NACA 0012 airfoil toward the target pressure distribution for the NACA 64A410 airfoil at $M_\infty = 0.735$, $\alpha = 0°$, and $C_l = 0.75$. This case requires a shift in the shock location and a significant change in the profile shape such that the target pressure distribution is obtained. The final solution almost exactly recovers the pressure distribution and the airfoil shape. In the next example, Figure 5, the NACA 0012 airfoil is again used as the starting condition to obtain the pressure distribution of the GAW72 airfoil operating at $M_\infty = 0.7$, $\alpha = -2°$, and $C_l = 0.57$. This case is difficult since the target airfoil has a cusped trailing edge while the initial airfoil has a finite trailing edge. As was seen in some of the non-lifting cases, there are small discrepencies evident near the trailing edge that may be due to the incomplete basis of the chosen design variables. The difference in the profiles between the final design and actual GAW72 is partly due to the fact that the GAW72 cordinates place the trailing edge at a non-zero y ordinate while the NACA 0012 places the trailing edge at $y = 0$. Also, the designed airfoil is subject to an arbritrary rotation since the angle of attack is free during optimization. The last test case in which the design program is run in inverse mode involves driving the NACA 0012 airfoil at $M_\infty = 0.75$ to obtain the target pressure distribution of the RAE airfoil at the same Mach number, $\alpha = 1.0°$, and $C_l = 0.80$. Due to the steep favorable pressure grardient at the leading edge upper surface and the strong shock exhibited (see Figure 6) by the RAE airfoil at these conditions this case represents quite a difficult test for the program. In the observed results, discrepencies are evident between the target and the final designed pressure distributions in both the leading and trailing edge regions. A comparison of the profiles reveals that the floating α in the design process has resulted in a rotation between the target and the final design. Looking at the final angle of attack of 0.74° which is slightly off the $\alpha = 1.0°$ of the target reveals that the rotation is compensated in large degree by the floating α. However, both airfoils have leading and trailing edges at 0.0; hence, the difference between the airfoils is not a simple rotation. This result, combined with an incomplete basis space, may account for the observed differences in pressure distributions.

The last group of results introduces drag as the cost function. Again the design process is carried out in the fixed lift mode. In Figure 7, the first drag minimization example, a NACA 0012 is again used as a starting airfoil. The design takes place at $M_\infty = 0.75$ and $C_l = 0.50$ where a strong shock causes considerable wave drag in the initial airfoil. To make the problem interesting, the optimization is carried out such that symetry of the design is perserved. The final design is a symetric airfoil with an increased maximum thickness that operates at the same lift coefficient, but has a reduction in drag from $C_d = 0.0127$ to $C_d = 0.0016$. In the final test case (see Figure 6) the camber distribution is optimized insted of thickness distribution. The design starts from a NACA 64A410 airfoil operating at $M_\infty = 0.75$, and $C_l = 0.60$ which displays 42 counts of drag according to the potential flow calculation. By allowing only changes to the camber distribution, a final airfoil is produced which maintains $C_l = 0.60$ but does so with only 4 counts of drag.

Conclusions and recommendations

We have developed a control theory based airfoil design method for a two-dimensional finite volume discretization of the potential flow equation. The method represents an extension of Jameson's previous work on the design of a conformally mapped airfoil. The new method is both efficient and robust, combining the versatility of numerical optimization methods with the efficiency of inverse design methods. The motivating factor behind this work is its direct extendability to three-dimensions. The ultimate goal of this effort is to create practical aerodynamic shape design methods for complete aircraft

configurations.

Acknowledgment

This work has benefited from the generous support of AFOSR under Grant No. AFOSR-91-0391 and also the support of the Advanced Aeronautical Concepts Branch of NASA Ames Research Center.

NCC 2-5012

References

[1] O. Baysal and M. E. Eleshaky. Aerodynamic design optimization using sensitivity anaysis and computational fluid dynamics. *AIAA paper 91-0471*, 29th Aerospace Sciences Meeting, Reno, Nevada, January 1991.

[2] P.E. Gill, W. Murray, and M.H. Wright. *Practical Optimization*. Academic Press, 1981.

[3] R. M. Hicks and P. A. Henne. Wing design by numerical optimization. *Journal of Aircraft*, 15:407–412, 1978.

[4] A. Jameson. Iterative solution of transonic flows over airfoils and wings, including flows at Mach 1. *Communications on Pure and Applied Mathematics*, 27:283–309, 1974.

[5] A. Jameson. Acceleration of transonic potential flow calculations on arbitrary meshes by the multiple grid method. *AIAA paper 79-1458*, Fourth AIAA Computational Fluid Dynamics Conference, Williamsburg, Virginia, July 1979.

[6] A. Jameson. Aerodynamic design via control theory. *Journal of Scientific Computing*, 3:233–260, 1988.

[7] A. Jameson. Automatic design of transonic airfoils to reduce the shock induced pressure drag. In *Proceedings of the 31st Israel Annual Conference on Aviation and Aeronautics, Tel Aviv*, pages 5–17, February 1990.

[8] V. M. Korivi, A. C. Taylor III, P. A. Newman, G. W. Hou, and H. E. Jones. An incremental strategy for calculating consistent discrete CFD sensitivity derivatives. *NASA TM 104207*, Langley Research Center, Hampton, VA, February 1992.

[9] M.J. Lighthill. A new method of two-dimensional aerodynamic design. *R & M 1111*, Aeronautical Research Council, 1945.

[10] J.L. Lions. *Optimal Control of Systems Governed by Partial Differential Equations*. Springer-Verlag, New York, 1971. Translated by S.K. Mitter.

[11] P. A. Newman, G. J.-W. Hou, H. E. Jones, A. C. Taylor III, and V. M. Korivi. Observations on computational methodologies for use in large-scale gradient-based, multidisciplinary design incorporating advanced CFD codes. *NASA TM 104206*, Langley Research Center, Hampton, VA, February 1992.

[12] O. Pironneau. *Optimal Shape Design for Elliptic Systems*. Springer-Verlag, New York, 1984.

[13] J. Reuther, C.P. van Dam, and R. Hicks. Subsonic and transonic low-Reynolds-number airfoils with reduced pitching moments. *Journal of Aircraft*, 29:297–298, 1992.

[14] G. R. Shubin. Obtaining cheap optimization gradients from computaional aerodynamics codes. *Internal paper AMS-TR-164*, Boeing Computer Services, June 1991.

[15] G. R. Shubin and P. D. Frank. A comparison of the implicit gradient approach and the variational approach to aerodynamic design optimization. *internal paper AMS-TR-164*, Boeing Computer Services, April 1991.

[16] S. Ta'asan, G. Kuruvila, and M. D. Salas. Aerodynamic design and optimization in one shot. *AIAA paper 91-005*, 30th Aerospace Sciences Meeting and Exibit, Reno, Nevada, January 1992.

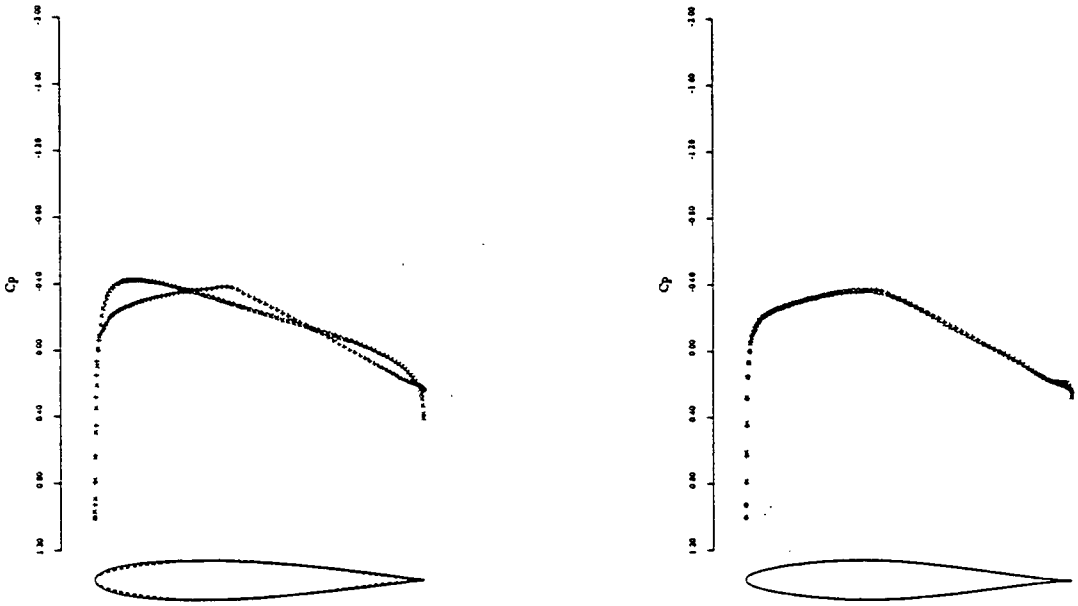

1a: Initial Condition
$C_l = 0.0000$, $C_d = 0.0001$

1b: 7 Design Iterations
$C_l = 0.0000$, $C_d = 0.0000$

Figure 1: Subsonic Non-Lifting Design Case, $M = 0.2$, $\alpha = 0°$.
—, × Initial Airfoil: NACA 0012.
- - -, + Target C_p: NACA 64012, $M = 0.2$.
Inverse Design

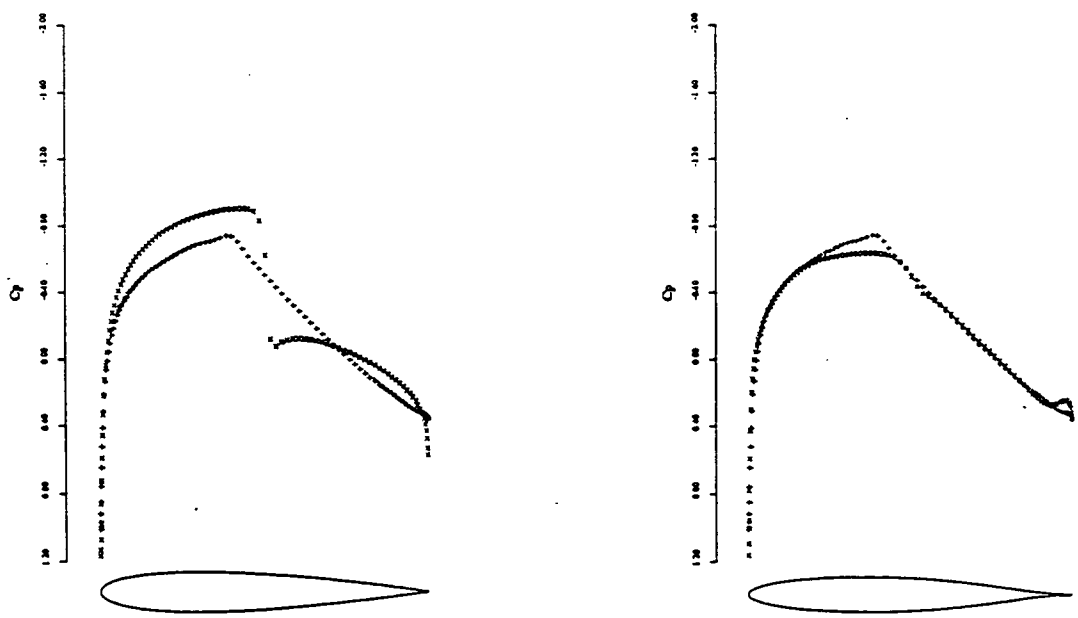

2a: Initial Condition
$C_l = 0.0000$, $C_d = 0.0063$

2b: 7 Design Iterations
$C_l = 0.0000$, $C_d = 0.0003$

Figure 2: Transonic Non-Lifting Design Case, $M = 0.8$ $\alpha = 0°$.
—, × Initial Airfoil: NACA 0012.
- - -, + Target C_p: NACA 64021, $M = 0.2$.
Inverse Design

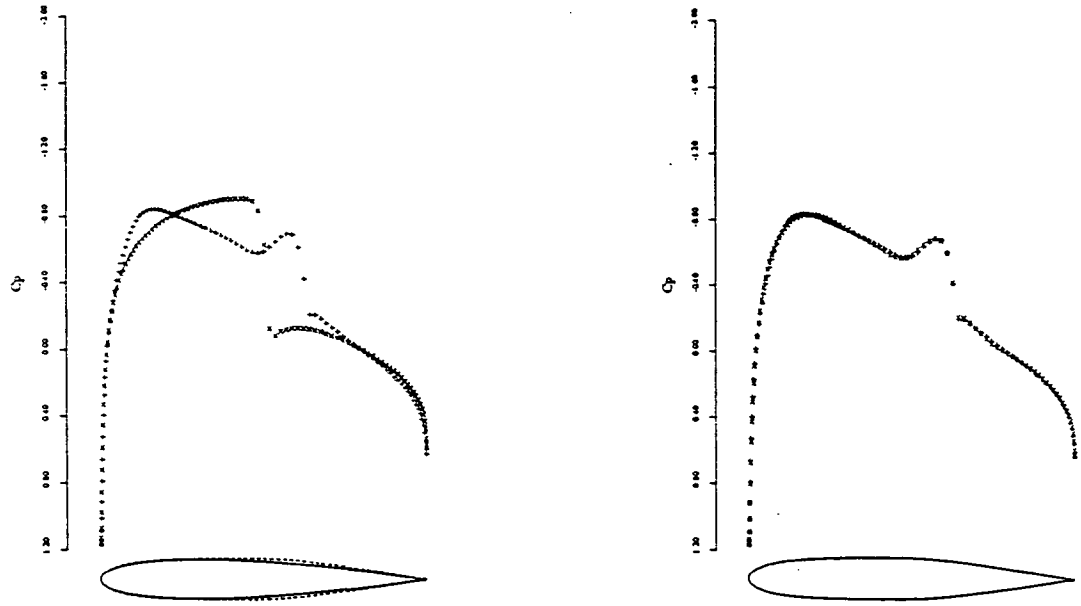

3a: Initial Condition
$C_l = 0.0000$, $C_d = 0.0063$

3b: 8 Design Iterations
$C_l = 0.0000$, $C_d = 0.0015$

Figure 3: Transonic Non-Lifting Design Case, $M = 0.8$, $\alpha = 0°$.
—, × Initial Airfoil: NACA 0012.
- - -, + Target C_p: NACA 64X, $M = 0.8$.
Inverse Design

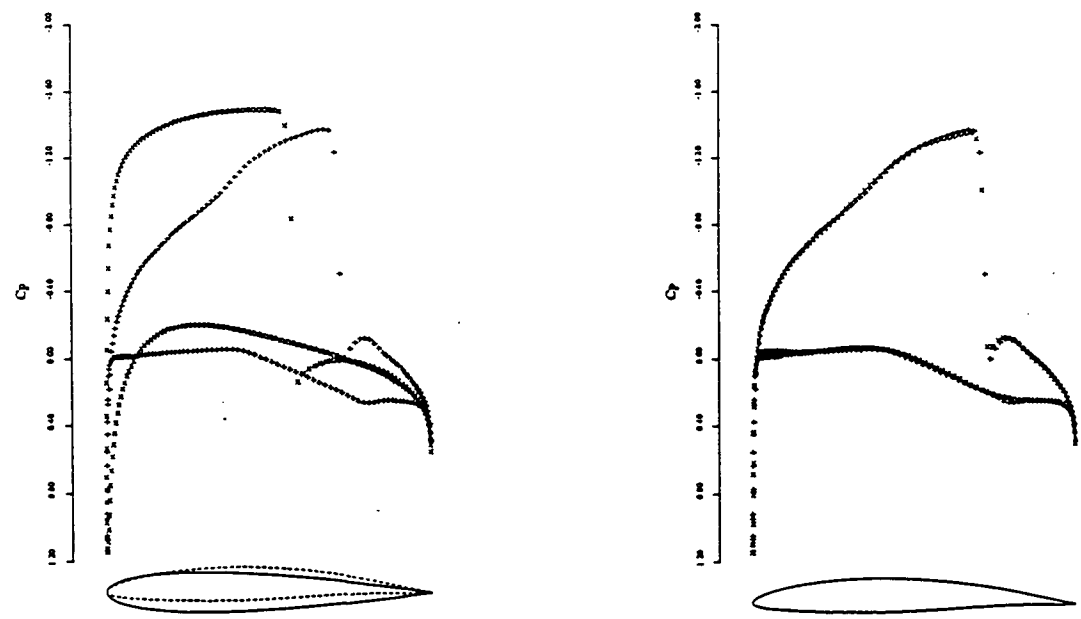

4a: Initial Condition
$C_l = 0.7315$, $C_d = 0.0252$, $\alpha = 2.664°$

4b: 20 Design Iterations
$C_l = 0.7334$, $C_d = 0.0086$, $\alpha = 0.032°$

Figure 4: Transonic Lifting Design Case, $M = 0.735$ Fixed Lift.
—, × Initial Airfoil: NACA 0012.
- - -, + Target C_p: NACA 64A410, $M = 0.735$, $C_l = 0.73$.
Inverse Design

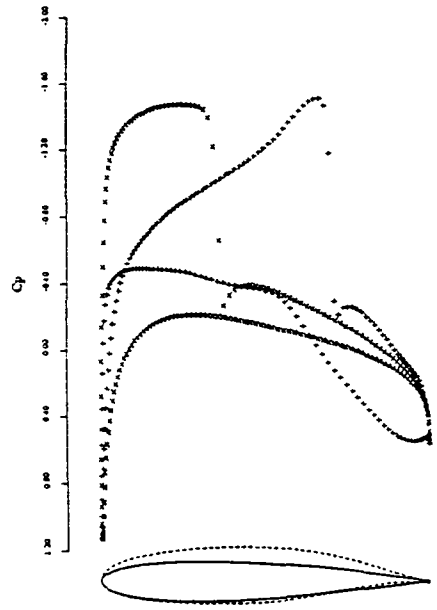

5a: Initial Condition
$C_l = 0.5492$, $C_d = 0.0047$, $\alpha = 2.709°$

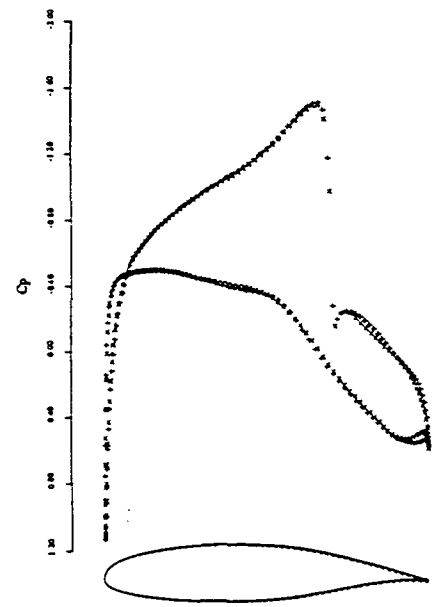

5b: 30 Design Iterations
$C_l = 0.5496$, $C_d = 0.0045$, $\alpha = -1.508°$

Figure 5: Transonic Lifting Design Case, $M = 0.70$, Fixed Lift.
—, × Initial Airfoil: NACA 0012.
- - -, + Target C_p: GAW72, $M = 0.70$.
Inverse Design

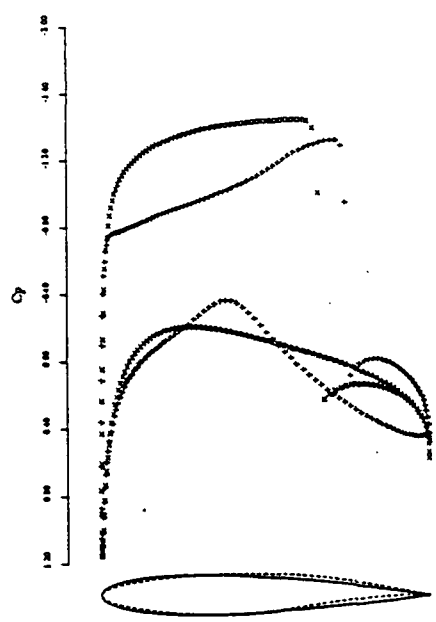

6a: Initial Condition
$C_l = 0.7946$, $C_d = 0.0358$, $\alpha = 2.364°$

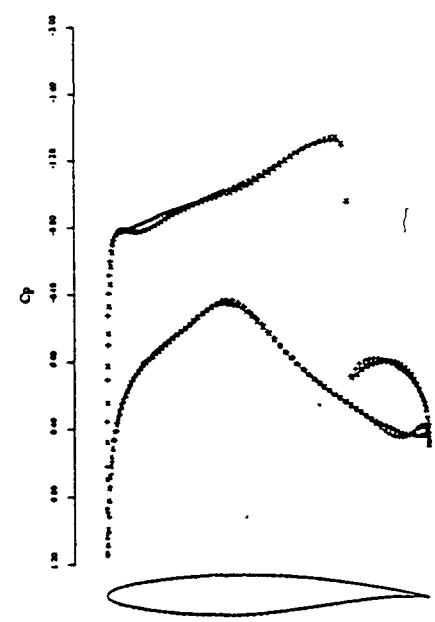

6b: 27 Design Iterations
$C_l = 0.7970$, $C_d = 0.0116$, $\alpha = 0.737°$

Figure 6: Transonic Lifting Design Case, $M = 0.75$ Fixed Lift.
—, × Initial Airfoil: NACA 0012.
- - -, + Target C_p: RAE, $M = 0.75$.
Inverse Design

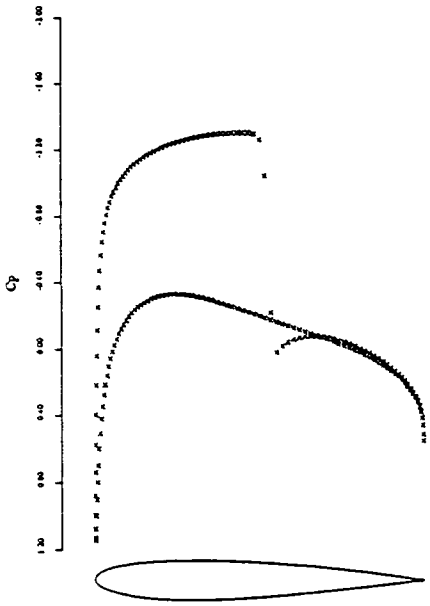

7a: Initial Condition
$C_l = 0.5037$, $C_d = 0.0127$, $\alpha = 1.856°$

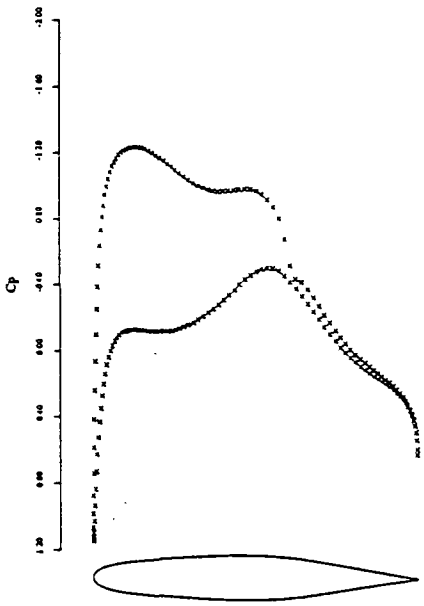

7b: 2 Design Iterations
$C_l = 0.5042$, $C_d = 0.0016$, $\alpha = 1.990°$

Figure 7: Transonic Lifting Design Case, $M = 0.75$, Fixed Lift.
—, × Initial Airfoil: NACA 0012.
Symetric Drag Minimization.

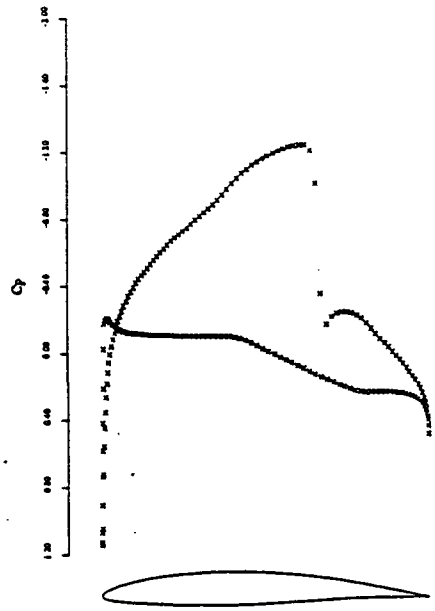

8a: Initial Condition
$C_l = 0.5964$, $C_d = 0.0042$, $\alpha = -0.464°$

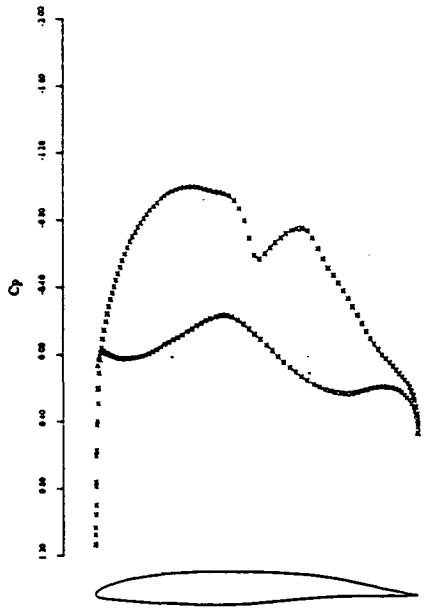

8b: 2 Design Iterations
$C_l = 0.5966$, $C_d = 0.0004$, $\alpha = 0.175°$

Figure 8: Transonic Lifting Design Case, $M = 0.735$ Fixed Lift.
—, × Initial Airfoil: NACA 64A410.
Camber Only Drag Minimization.